UCRL- 84380
PREPRINT
CONF-7908139--1

SOME RECENT EFFORTS TOWARD HIGH DENSITY IMPLOSIONS

MASTER

Gene E. McClellan

THIS PAPER WAS PREPARED FOR THE

Gordon Conference on Laser Interaction
with Matter - Tilton, New Hampshire,
August 13, 1979

December 4, 1980

Lawrence Livermore Laboratory

1. Some recent Livermore efforts towards achieving high density implosions are presented. The implosion dynamics necessary to compress DT fuel to 10 to 100 times liquid density are discussed. Methods of diagnosing the maximum DT density for specific designs are presented along with results to date.

2. Specific contributors to this talk are listed in Fig. 2.

3. The Livermore Laser Fusion Program has made steady progress in achieving high density implosions with the SHIVA Laser. The best results to date are DT implosions to densities in the 50 to 100 times liquid density range.

Recently, we have turned attention to some simple designs which we will discuss here. (Latest results to be plotted on Fig. 3.)

4. In an exploding pusher, the fuel is preheated by suprathermal electrons and shocked to a high temperature before being adiabatically compressed. The resulting high temperature implosion to approximately liquid DT density gives the highest neutron yield for present lasers. However, efficient reactor designs for future lasers require that the bulk of the DT fuel be compressed to densities of order 1000 times liquid density before thermonuclear ignition. Targets must be designed to reduce both preheat and initial shock heating so that the compression approaches the Fermi degenerate adiabat.

5. A thicker pusher reduces suprathermal preheat. The ablation-driven shock causes the fuel to be driven by denser, cooler pusher material, resulting in compression to higher density. A problem exists for some combinations of preheat and pusher thickness. If thermal expansion of the inside of the pusher compresses and stagnates the fuel before the ablation driven shock has time to penetrate the pusher, then pusher/fuel mixing may degrade target performance.

6. The worst case mix assumption is that some of the pusher material penetrates the fuel at the highest interface velocity and that when about half of the fuel mass has been penetrated, all thermonuclear reactions stop. Better estimates can be made using the theory of the Rayleigh-Taylor fluid instability.

7. The target ball, the laser illumination scheme, and the 1-D simulation results for the SHIVA 10X design are shown in Fig. 7.

8. The target ball and the 1-D simulation results for the SHIVA 100X design are shown in Fig. 8.

9. Three methods of diagnosing the compressed fuel density for 10-100X implosions that will be discussed are x-ray imaging of the pusher material, line emission imaging of the seeded fuel, and radiochemistry measurements of neutron activation.

10. The pusher material may be imaged by its own x-ray emission or by backlighting with an external source of x-rays. Backlighting becomes useful for high density implosions when self-emission is reduced by lower temperature and increased pusher ρR.

11. Exploding pushers are thin to most x-rays and charged particles, so a good estimate of compression can be obtained with several imaging techniques. Figure 11 shows densitometer traces from images of 2 keV x-rays, 20 keV x-rays, argon He-α emission, and 3.5 meV alpha particles.

12. For intermediate density targets, 2 keV x-rays cannot be used to see through the thick pusher to the fuel/pusher interface. Imaging of higher energy x-rays is required. Location of the interface is uncertain.

13. Figure 13 discusses some uncertainties in the interpretation of x-ray images.

14. Figure 14 (in one or more parts) will show x-ray microscope images of the 10X and 100X SHIVA experiments and estimates of the compressed fuel volume will be made.

15. With about 1% atomic fraction of argon in the DT fuel, the image of the argon line emission can be used to determine the size of the

compressed core. Only one spatial dimension is imaged in our spectrometer. The conditions for an observable image are listed.

16. Corrections to go from the size of the observed argon line image to the size of the fuel region are moderate for the 10X design. The largest uncertainty is in the optical depth of the emission region at the argon line. There is about a 30% difference in observed radius between the optically thin and thick cases.

17. Densitometer traces of 1-D images from experiment and calculation are shown. Using the sphericity taken from x-ray microscope images, a fuel density is quoted.

18. Radiochemical activation of the pusher or a seed material in the fuel by thermonuclear neutrons determines $\rho\Delta R$ at "burn" time. A diagram and typical nuclear reactions are shown in Fig. 18. We have measured pusher $\rho\Delta R$ with the Si reaction.

19,20. Assuming that the material to be activated is always in a thin shell adjacent to the DT fuel, the final DT density varies as the final pusher $(\rho\Delta R)^{3/2}$. This result is derived in Figs. 19 and 20. Significant model dependence is introduced in this relationship if part of the activated material is ablated during the implosion.

21. One dimensional (spherically symmetric) model dependence in the relation between fuel density and measured pusher $\rho\Delta R$ are introduced by variations in burn/compression times and in final state density profiles. The thermonuclear reactions are quenched by electron conduction to the cool pusher before maximum fuel density is attained. The amount by which the fuel is compressed after "burn" must be gotten from model dependent calculations. Preheat and ablation details also introduce uncertainty in the density profile of the glass at "burn;" however, if the glass ΔR is small, then $\rho\Delta R$ will not be effected.

22. Delete.

23. Two-dimensional effects arise through assymmetry and fluid instability mixing of pusher and fuel materials.

24. Fig. 24 shows a plot of peak fuel density vs. pusher $\rho\Delta R$ for various preheat and absorbed energy assumptions for the 10X target design. Upper and lower limits on fuel density are given by the "no mix" and "extreme mix" assumptions for the 1-D calculations. An unreasonably extreme lower limit is obtained by assuming that the glass is in pressure equilibrium with the fuel, but is Fermi degenerate. The measured $\rho\Delta R$ of 0.0036 g/cm^2 implies a peak DT density between 4 and 10 times liquid density. (The same result for the 100X design will be presented if available.)

25. Delete.

26. Fig. 26 presents a summary of the experimental results for the 10X target design. (Similar results for the 100X design will be presented if available.)

27. A double-shelled target with an exploding outer shell is being considered as a means to reduce fuel/nuclear preheat and smooth the absorption assymmetry associated with two-sided laser illumination. (See UCRL 81327 and 1978 Laser Fusion Annual Report, Sections 3.3 and 5.7 of unclassified report.) A thick, ablatively-driven outer shell would not improve implosion symmetry.

28. The inner ball of the double-shelled target is ablated first by hot electrons produced in the outer shell. Then a strong shock is generated by the impact of the outer shell material. A typical radius-time plot is shown.

29. The transition from single shell to double shell dynamics can be viewed by plotting target performance versus shell separation. In the limit of zero separation, a single shell target is obtained. For small separations, the final fuel density is constant, but less efficient use of energy causes the 1-D yield to drop. As the shell separation increases, there is time to store energy in the outer shell material and

then deliver it to the inner shell as a second shock. The resulting implosion goes to higher density than the single shell target.

30. The primary goal of the exploding outer shell is to symmetrize the pressure applied to the ablator pusher by electron conduction and hydrodynamic flow. The flow of material from the poles of the outer shell (region of best laser abosrption) to the equator of the inner ball is evident in 2-D simulations of the implosion.

31. A unique visualization of the hydrodynamic flow was obtained in our first SHIVA experiment with double-shelled targets. X-ray images in the 1 to 2 KeV range showed a ring shock around the equator of the inner ball formed by the stagnation of the inward-flowing material. A comparison with calculation is shown.

32. The experiments (2) gave below-threshold neutron yields, so the goal of 50X density was probably not achieved. A low absorption on CH at 2×10^{15} W/cm^2 and 1 ns FWHM could be the reason. Target performance versus laser absorption is shown.

33. Another difficulty may be the generation of strong nx T magnetic fields between the two shells. The fields prevent symmetrization by electron conduction, but have negligible effect on the hydrodynamic flow discussed earlier.

34. To improve laser absorption and reduce the effects of magnetic fields, we went to 200 ps, a 2:1 radius ratio, and a thinner inner ball. Two shots gave almost equal yields. 2-D simulations with magnetic fields alone or reduced flux limits alone give neutron yeilds a factor of 50-100 too high. Magnetic fields with the two-stream mechanism of conduction inhibition reproduce the observed yield. Mix of pusher and fuel has been calculated to be negligible.

35. Delete.

36. We are looking for ways to reduce magnetic field effects. One way is to reduce initial temperature gradients by changing the shape (shimming) the outer shell to absorb laser energy more uniformly. An example is shown. The asymmetry introduced by the shimming must be overcome with hydro flow and conduction. Calculations are underway to see if magnetic fields are reduced sufficiently to provide net symmetrization.

37. Test calculations of shimmed exploding pushers are shown. The imploded shape is sensitive to the laser illumination profile, but the neutron yield is not since it depends mainly on absorbed power.

38. The design considerations for a diagnosable implosion to 10-100X liquid density are listed.

39. Some near-term improvements that can be pusued for achieving higher density implosions.

40. A summary of the subjects of the talks are listed.

Blank

SOME RECENT EFFORTS TOWARD HIGH DENSITY IMPLOSIONS

- 10-100 X implosion dynamics
- Design examples
- Diagnosis of intermediate density
- Results to date

50-90-0779-2245

Figure 1

CONTRIBUTORS TO THIS WORK

J. H. Nuckolls

J. T. Larsen

G. E. McClellan

W. C. Mead

C. D. Orth

Y. L. Pan

Figure 2

FUEL DENSITY AT BURN TIME VERSUS NEUTRON YIELD

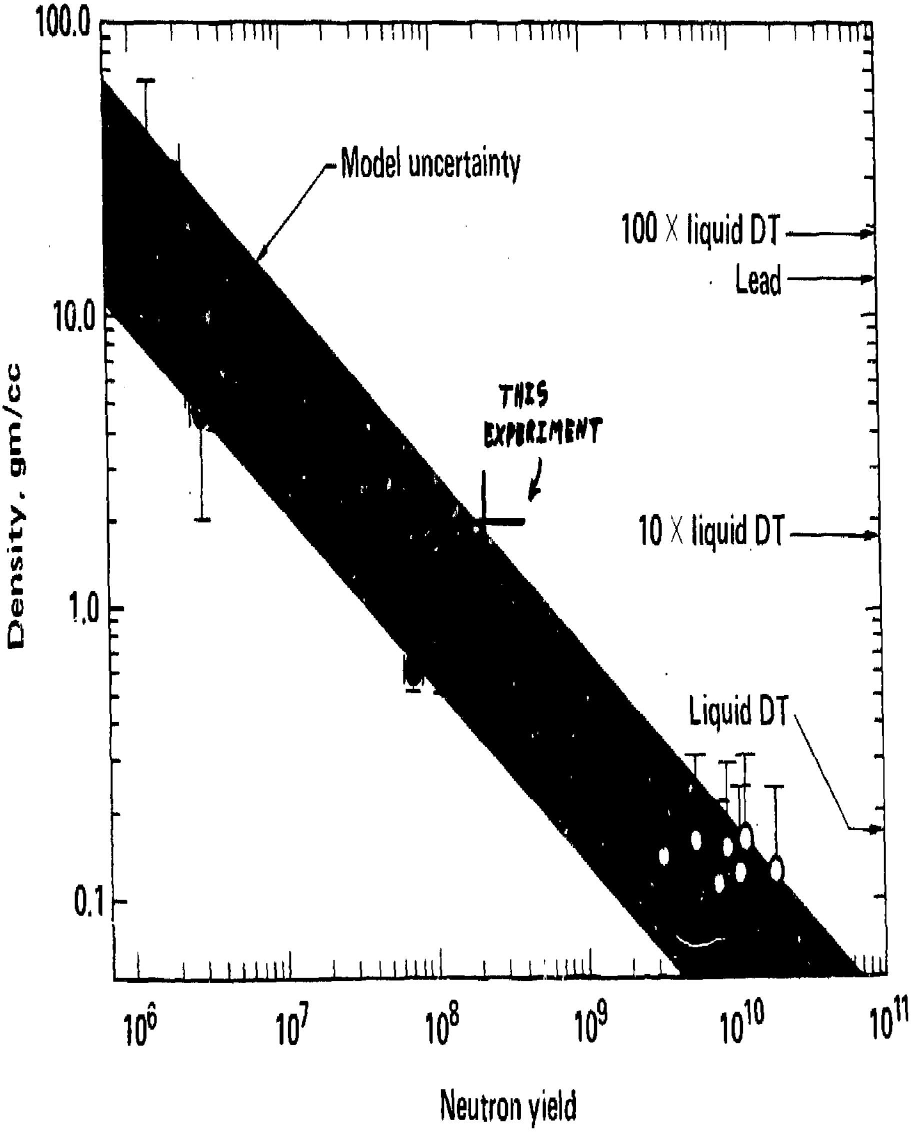

20-15-0579-1727

Figure 3

DT ADIABATS FOR 10-100 X TARGET DESIGNS

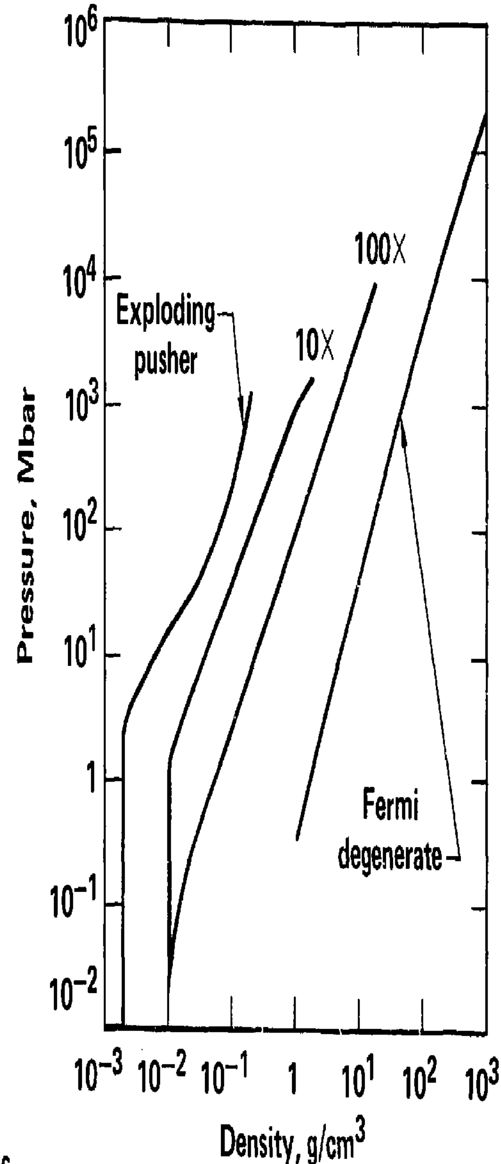

50-60-0779-2246

Figure 4

REDUCE PREHEAT AND IMPROVE FUEL AND PUSHER ADIABATS BY THICKENING THE PUSHER

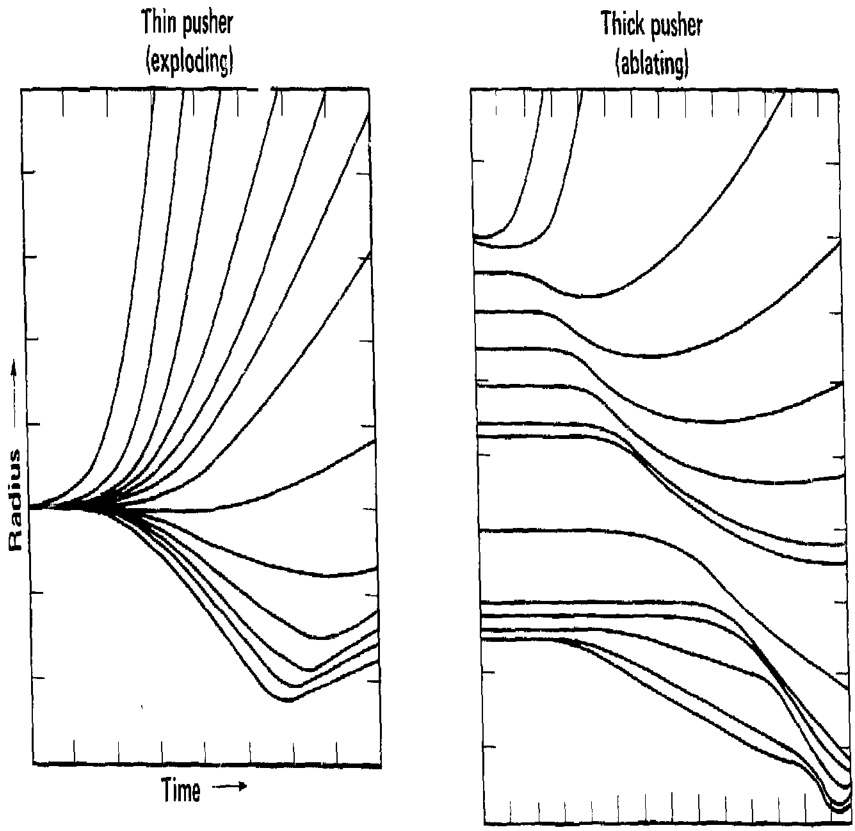

Implosion timing deteriorates if $R/V_{preheat} < \Delta R/V_{shock}$

50-60-0779-2261

Figure 5

WORST CASE MIX ASSUMPTION IS THAT SOME OF PUSHER MATERIAL PENETRATES FUEL AT HIGHEST INTERFACE VELOCITY

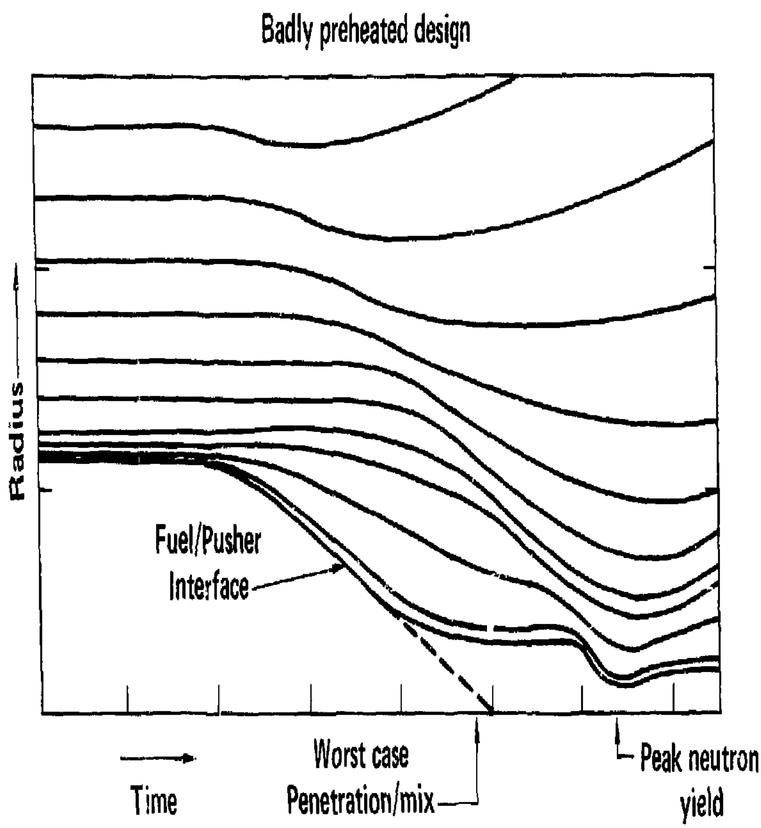

Stop thermonuclear reactions when ~ 50% of fuel mass is penetrated

50-60-0779-2260

Figure 6

10 X DESIGN FOR SHIVA

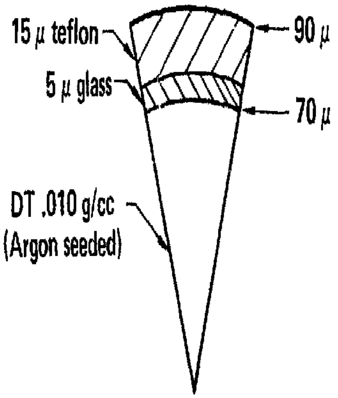

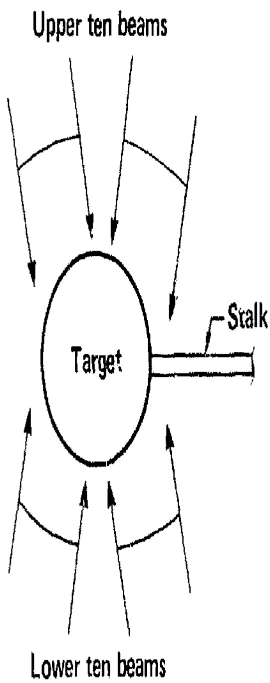

1-D calculation for SHIVA

Laser: 200 ps FWHM gaussian
4 kilojoules, 17% absorbed
$f_{hot} \sim 90\%$, $T_{hot} \sim 35$ keV

	No mix	Extreme mix
Yield:	4×10^8	2×10^8
Density:	16 X	4 X

02-30-0779-2243

Figure 7

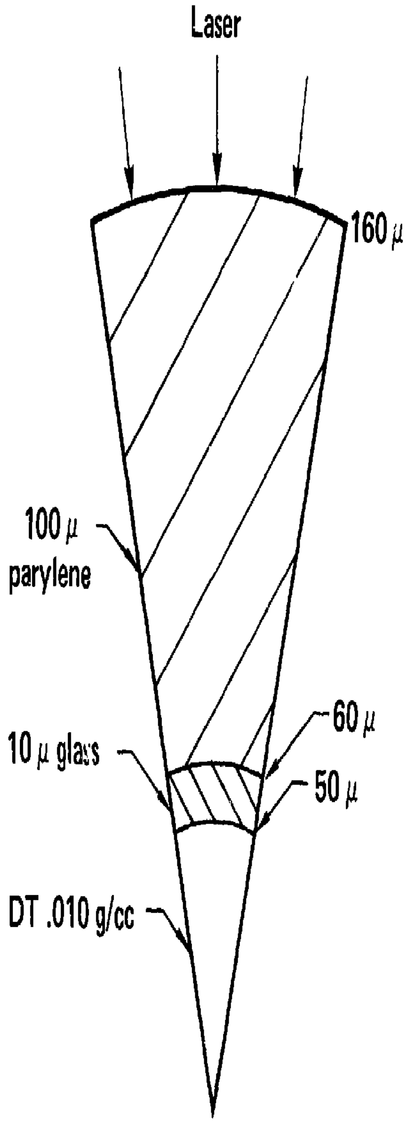

1-D calculation for SHIVA

Laser: 200 ps FWHM gaussian

4 kilojoules, 21% absorbed

$f_{hot} \sim 93\%$, $T_{hot} \sim 21$ keV

	No mix	Extreme mix
Yield	7×10^7	5×10^6
Density	130 X	80 X

02-30-0779-2242

Figure 8

METHODS OF DIAGNOSING INTERMEDIATE DENSITIES (10–100 X)

- X-ray imaging of pusher material
- Line emission imaging of seeded fuel
- Radiochemistry – measurement of neutron activation

50-60-0779-2247

Figure 9

PUSHER MATERIAL MAY BE IMAGED BY ITS OWN EMISSION OR WITH AN EXTERNAL SOURCE OF X-RAYS

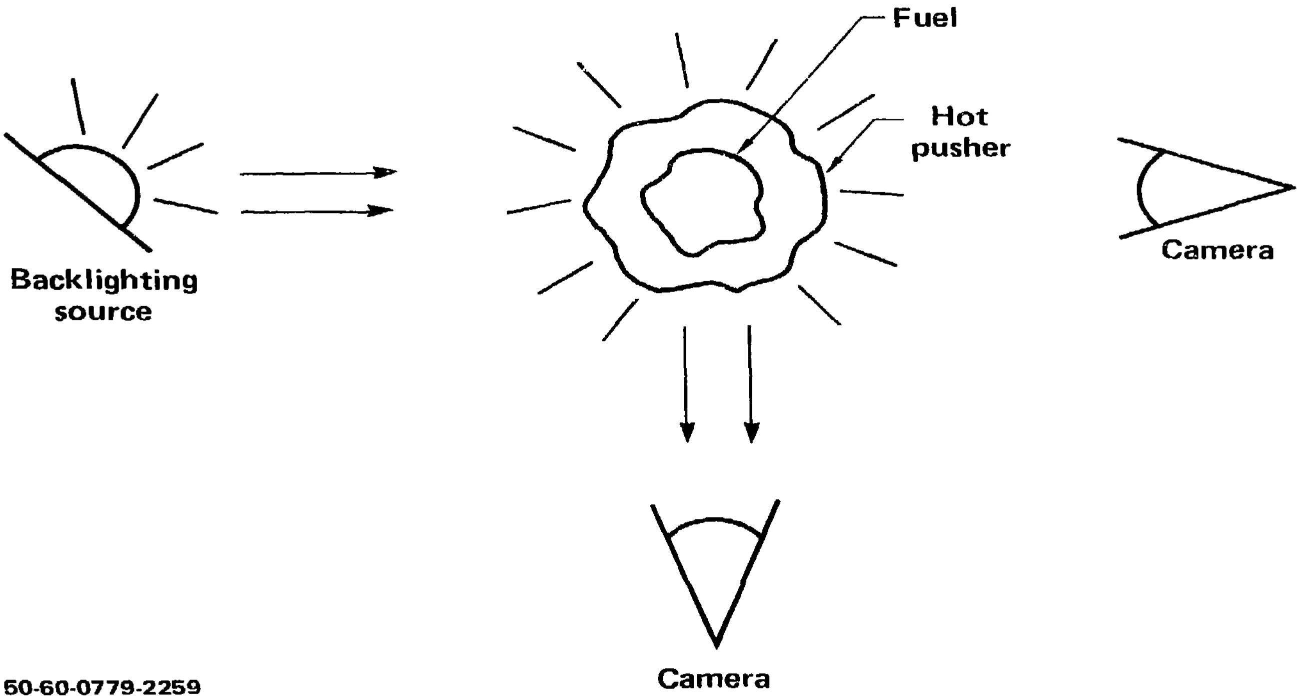

50-60-0779-2259

Figure 10

EXPLODING PUSHERS ARE THIN TO MOST X-RAYS AND CHANGED PARTICLES – HENCE A GOOD ESTIMATE OF COMPRESSION IS OBTAINED

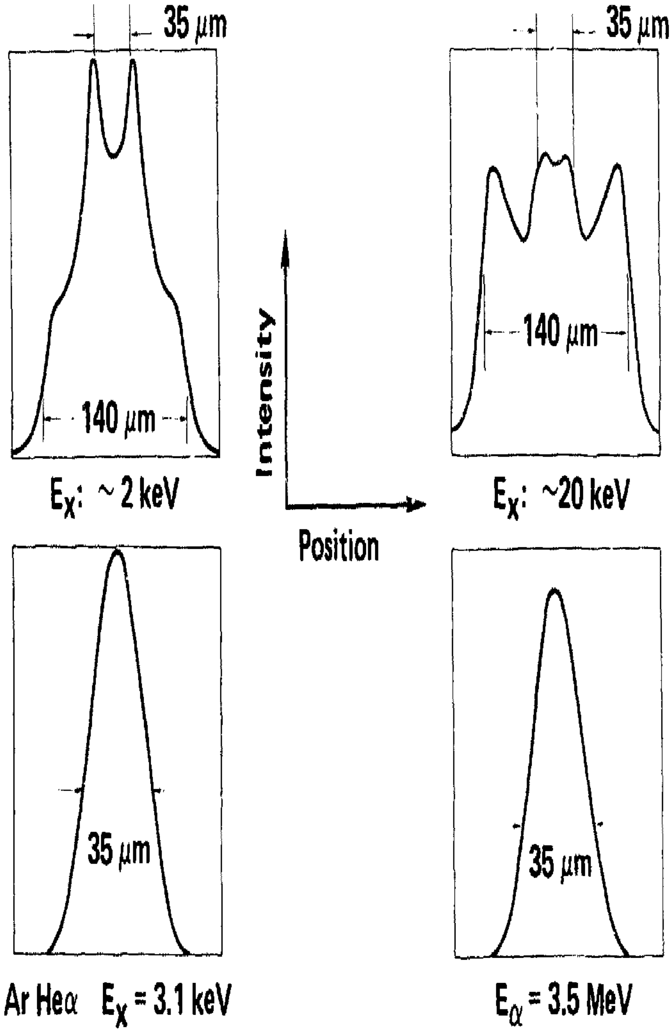

50-60-0779-2230

Figure 11

INTERMEDIATE DENSITY TARGETS HAVE THICK PUSHERS

- Compressed glass $\rho\Delta x$ is several times the intial $\rho\Delta x$
- For $E_x \approx 2$ keV, $K\rho\Delta x \gg 1$ and thus low energy x-rays are a poor diagnostic

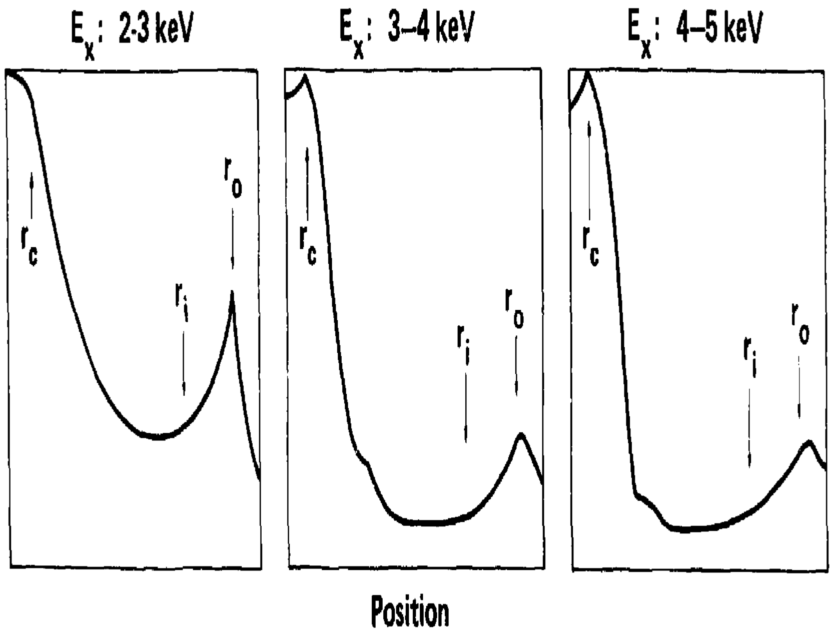

50-60-0779-2231

Figure 12

XRAY IMAGING OF COMPRESSED FUEL VOLUME IS USEFUL FOR SOME TARGET DESIGNS

- Low energy emission from pusher is dominated by free–bound processes – interprestation may be sensitive to pusher density and temperature behavior

- High energy pusher emission generated by bremstrahlung from superthermal electrons – samples density behavior of pusher

- Low energy line emission from trace gas in fuel depends on fuel temperature history – specific lines may be sensitive to absorption

50-60-0779-2229

Figure 13

Blank

2.5-4.5 keV PUSHER IMAGE ECCENTRICITY IS $\epsilon = 1.73 \pm 0.17$

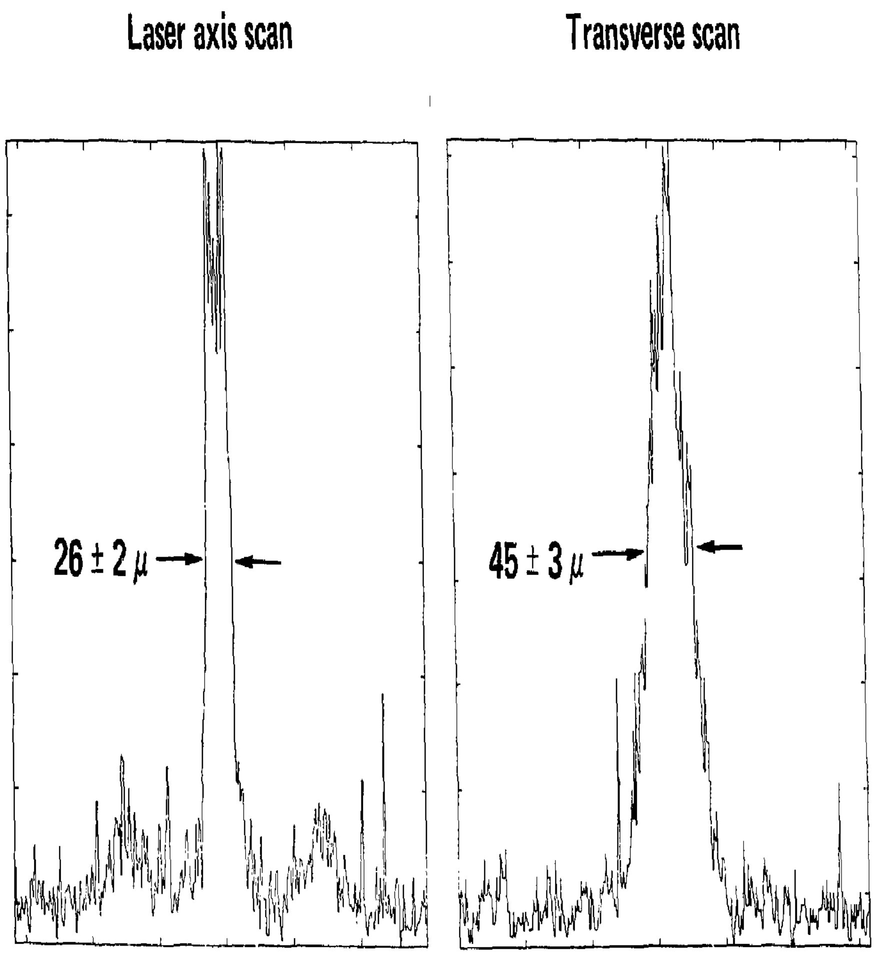

50-60-0180-0275

Figure 14A

USE 2-D NUMERICAL SIMULATION TO RELATE THE DT FUEL ECCENTRICITY AT BURN TIME TO THE OBSERVED PUSHER ECCENTRICITY

- Simulation result:

$$\frac{\epsilon_{DT}}{\epsilon_{pusher}} = 1.0 \pm 0.1$$

- X-ray microscope measurement of ϵ_{pusher} implies:

$$\epsilon_{DT} = 1.73 \pm 0.20$$

- Lower limit to fuel density at burn time is:

$$\rho_{DT} > 2.5 \times \text{Liquid density}$$

50-60-0180-0276

Figure 14B

IMAGE OF Ar LINE EMISSION FROM COMPRESSED CORE ALLOWS DENSITY DETERMINATION

Compressed core

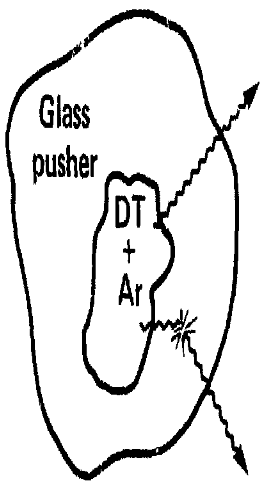

- Background

  Si free-bound

  Corona emission

  $I_b \sim 3 \times 10^{15}$ keV/keV

Imaging spectrometer

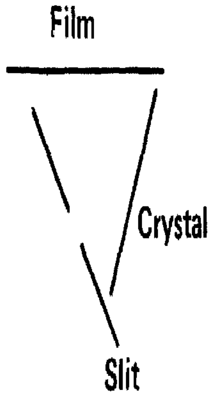

- He-like Ar excited at stagnation

  $T_e \sim 0.6\text{-}1.0$ keV

  $N_e \sim 10^{23}\text{-}10^{24}\ \text{cm}^{-3}$

  $I_0 \sim 10^{16}$ keV/keV

- Transport through pusher

  Si K-shell bound-free

  $\rho r)_{SiO_2} \sim 0.005\ \text{g/cm}^2 \Rightarrow$

  $5 - 15 \times$ attenuation

  $I_s \lesssim 2 \times 10^{15}$ keV/keV

50-60-0779-2250

Figure 15

CORRECTIONS TO SIZE OF Ar LINE IMAGE ARE MODERATE FOR SHIVA 10 X IMPLOSIONS

Variations of source optical depth leads to
$\lesssim$ 30% uncertainty in radius determination

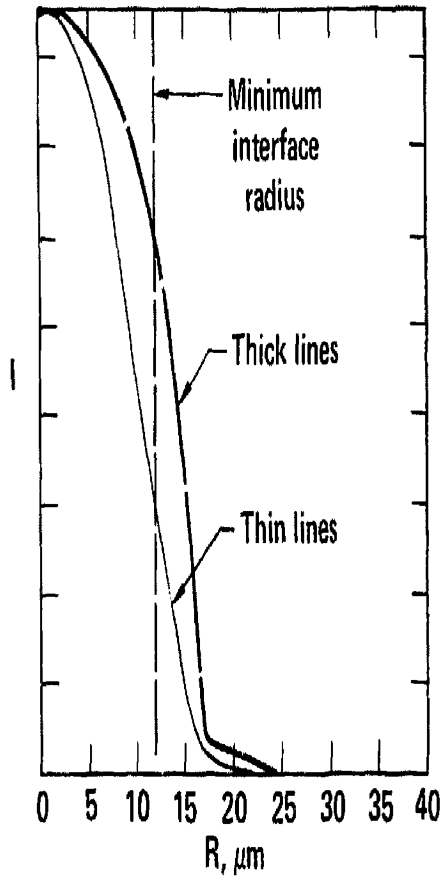

Implosion sphericity must be determined

Gross dynamical changes required to alter relative sizes of Ar emission/DT core

02-30-0779-2244

Figure 16

20 μ SLIT WIDTH MUST BE FOLDED WITH SOURCE TO GIVE IMAGE TO COMPARE WITH EXPERIMENT

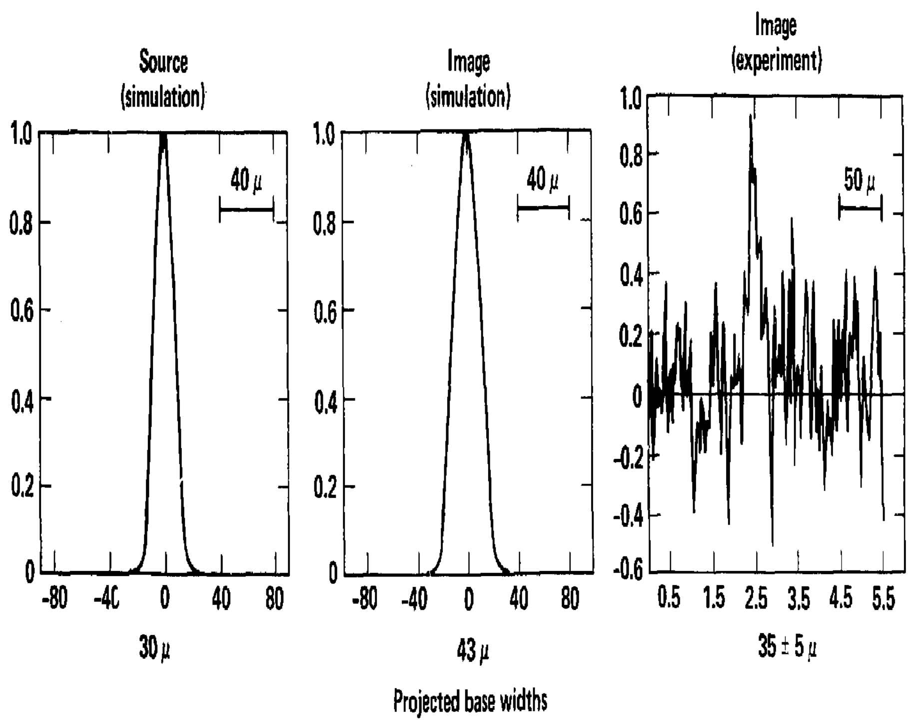

50-60-0180-0277

Figure 17A

A FUEL DENSITY OF (5^{+6}_{-2}) TIMES LIQUID DENSITY IS IMPLIED AT BURN TIME

- Argon line source diameter (axial) is $19 \pm 3\ \mu$
- Eccentricity from x-ray microscope 1.73 ± 0.20
- Initial fuel $136\ \mu$ diameter, 8.8 mg/cc
- Fuel density at burn time:

$$\rho_{DT} = 1.1^{+1.2}_{-0.5}\ \mathrm{g/cm^3}$$

50-6000180-0274

Figure 17B

RADIOCHEMICAL ACTIVATION OF PUSHER OR SEED MATERIAL DETERMINES ρR AT "BURN" TIME

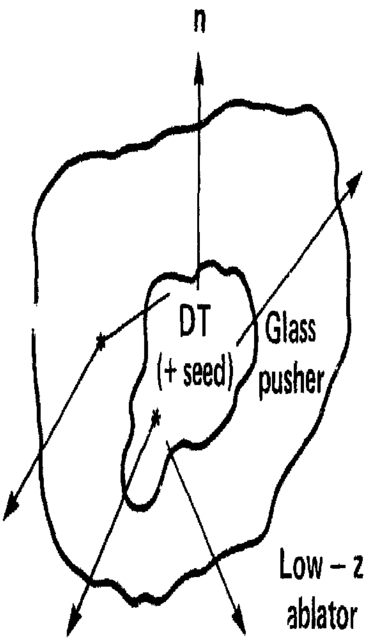

Reactions

- Pusher

$$^{28}Si + n \to \boxed{^{28}Al} + p \quad \to (^{28}Si, \beta, \gamma)$$

Diagnostic threshold: $N\,\rho R)_p \sim 10^5$

- Fuel seed

$$^{79}Br + n \to \boxed{^{78}Br} + 2n \quad \to (^{78}Se, \beta^+)$$

Diagnostic threshold: $N\,\rho R)_f \sim 3.10^5$

$$\frac{\text{Activation yield}}{\text{Neutron yield}} \sim \rho R)_{EFF} \sim n\tau$$

50-60-0779-2251

Figure 18

IN SIMPLEST MODEL, FINAL DT DENSITY VARIES AS FINAL PUSHER $(\rho\Delta R)^{3/2}$

- Assume thin shells at constant density, both initial and final
- Assume instantaneous burn at peak density

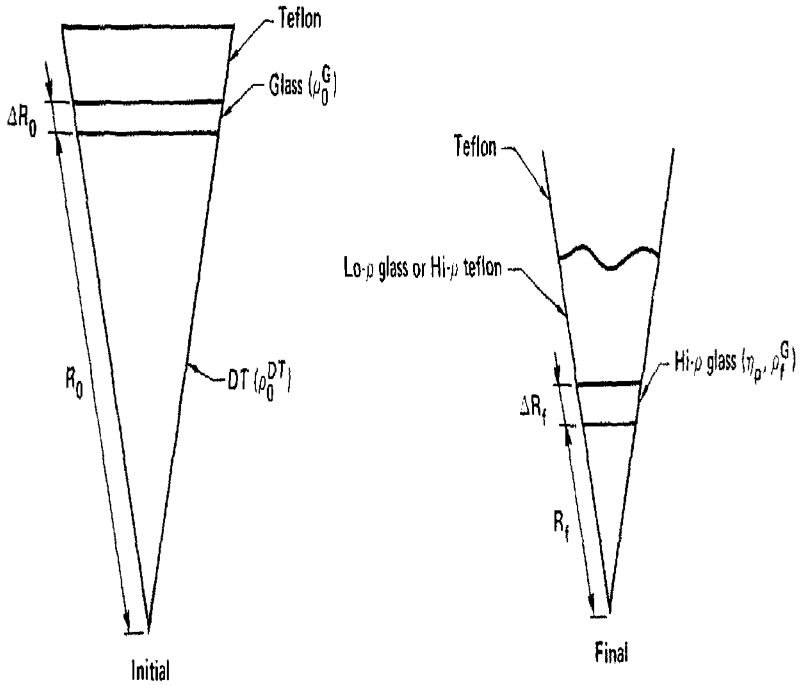

- Assume unablated glass fraction $\eta_p \equiv M_f^G/M_0^G$

50-60-0779-2249

Figure 19

EQUATE INITIAL AND FINAL MASSES TO OBTAIN RADIAL CONVERGENCE AND FINAL DENSITY

$$4\pi R_f^2 \rho_f^G \Delta R_f^G = \eta_p 4\pi R_0^2 \rho_0^G \Delta R_0^G$$

$$\text{Convergence:} \quad \frac{R_0}{R_f} = \left[\frac{(\rho\Delta R)_f^G}{\eta_p (\rho\Delta R)_0^G}\right]^{1/2}$$

$$\text{Density:} \quad \rho_f^{DT} = \left(\frac{R_0}{R_f}\right)^3 \rho_0^{DT} = \left[\frac{(\rho\Delta R)_f^G}{\eta_p (\rho\Delta R)_0^G}\right]^{3/2} \rho_0^{DT}$$

Cleanest result if $\eta_p = 1$

50-60-0779-2252

Figure 20

I-D MODEL DEPENDENCE ARISES THROUGH VARIATIONS IN BURN/COMPRESSION TIMES AND CHANGES IN FINAL STATE DENSITY PROFILES

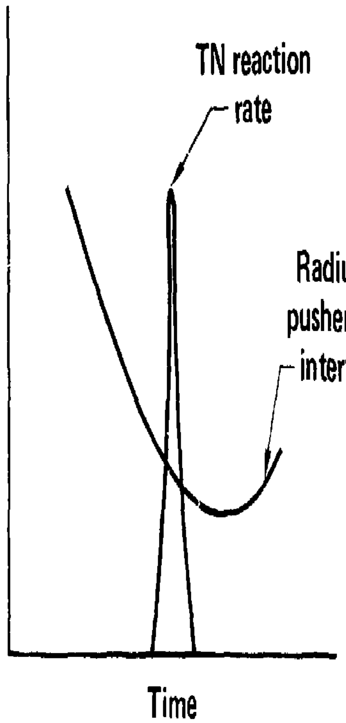

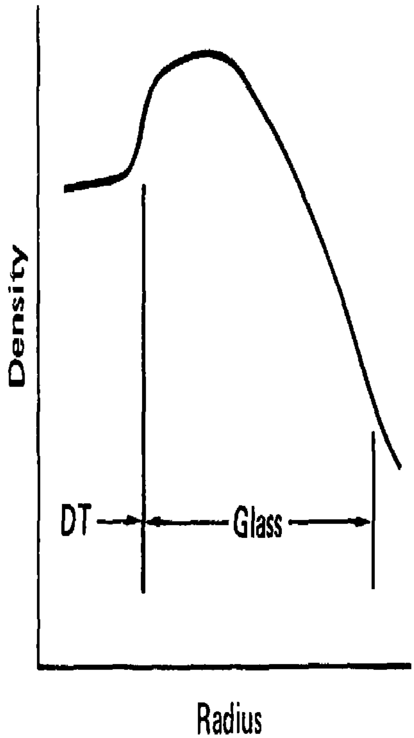

Fuel heating rate $\alpha\ P \frac{dV}{dt}$

Fuel cooling rate $\alpha\ K_e \nabla T_e$

Preheat/ablation/convergence

Determine final density profiles

Figure 21

2-D EFFECTS ARISE THROUGH ASYMMETRY AND FLUID-INSTABILITY/MIXING OF PUSHER/FUEL

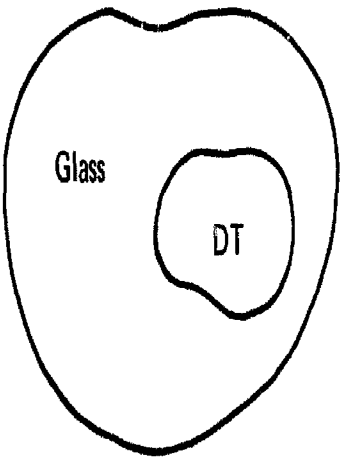

Simulations to be done
Est. to be insignificant

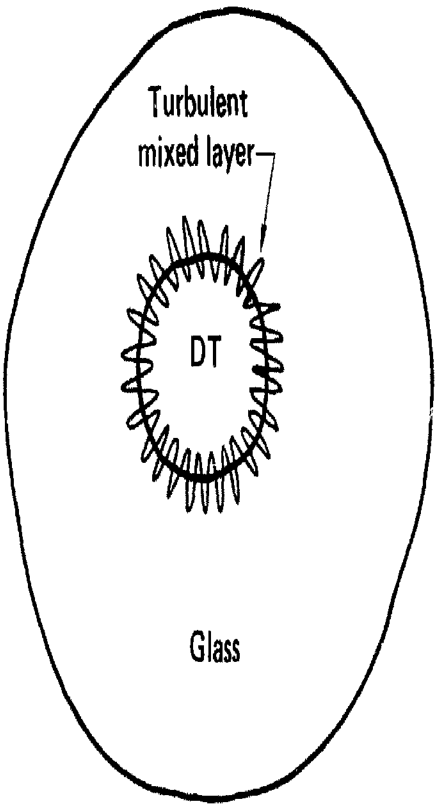

Calculations in progress
Possible 50% mix

50-60-0779-2253

Figure 23

MEASURED $\rho R)_{eff}$ FOR SHIVA "10X" TARGET IMPLIES 5-15X LIQUID DENSITY

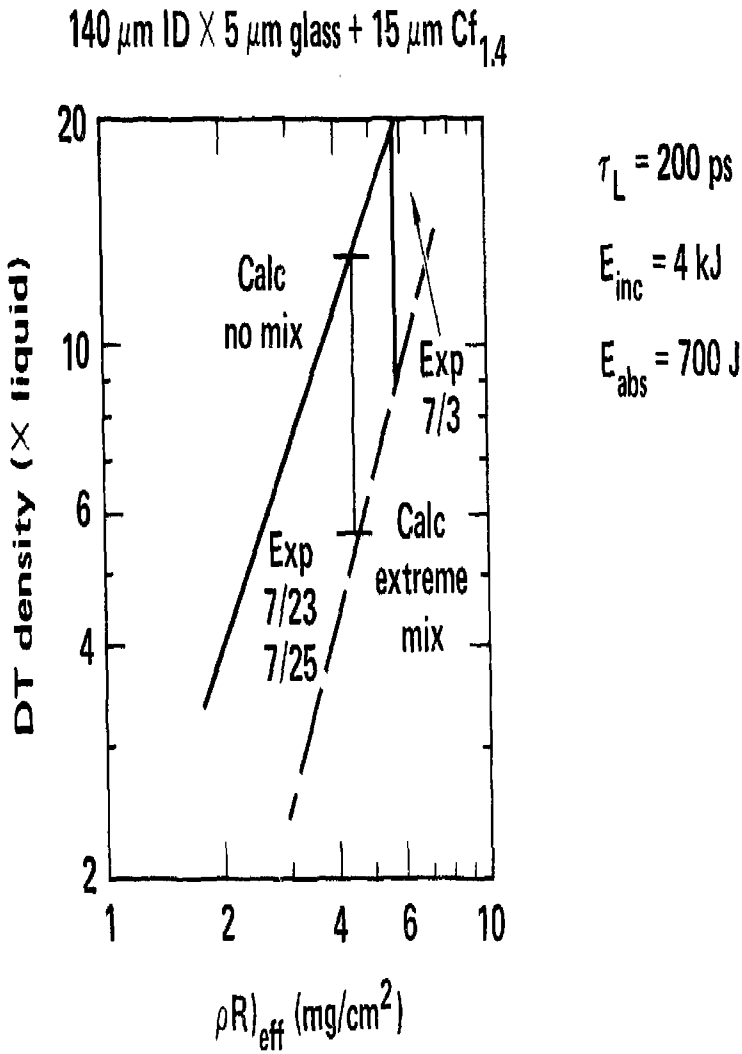

02-30-0180-0273

Figure 24A

TARGET PREHEAT AND DRIVE DEPEND UPON THE SUPERTHERMAL ELECTRON TEMPERATURE AND ABSORPTION

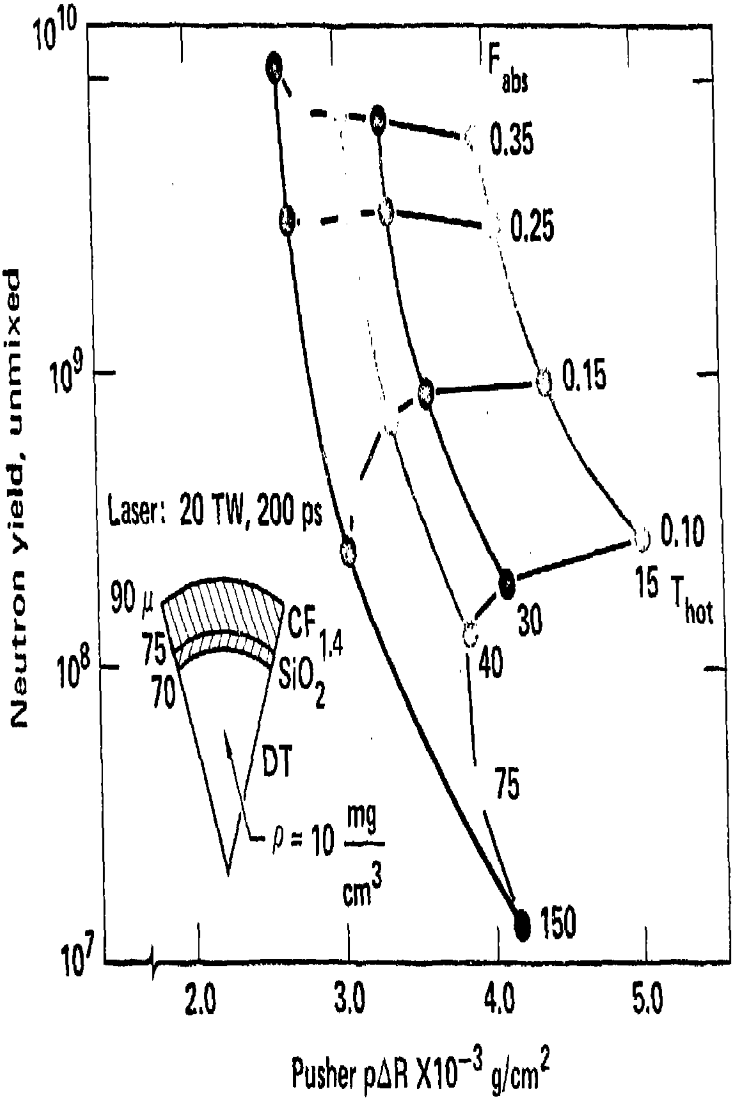

50-60-0879-2394

Figure 24B

SUMMARY OF RESULTS FOR THE SHIVA 10X TARGET

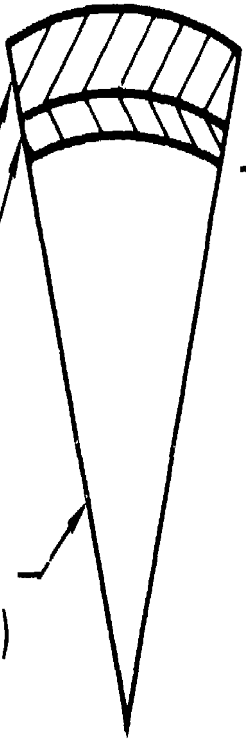

4 kJ, 200 ps FWHM

(3 - 7) X 10^8 neutrons

X-ray image:	$\rho_{DT} > 2.5$ X	eccentricity ~ 1.7
Argon line image:	(5^{+6}_{-2}) X	at burn time
Radiochemistry:	5-15 X	peak density

02-30-0180-0272

Figure 26

DOUBLE SHELLED TARGET WITH EXPLODING OUTER SHELL

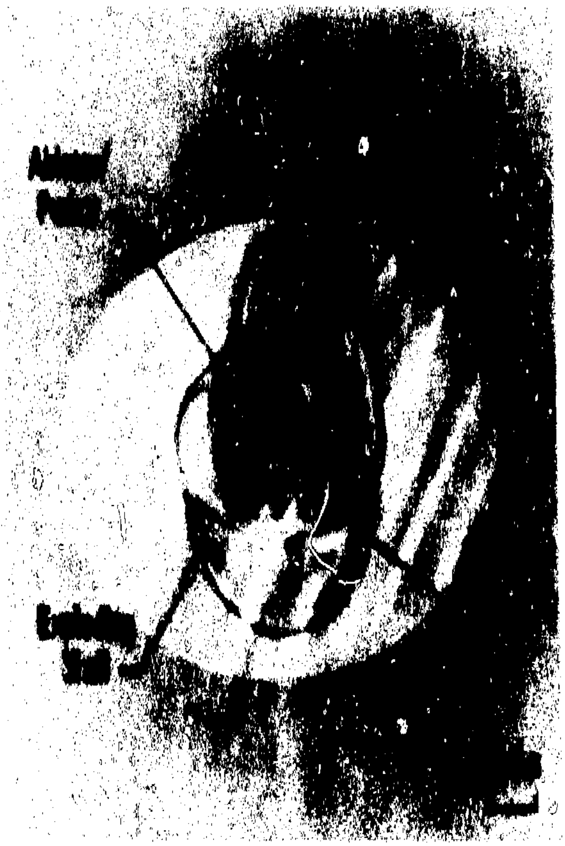

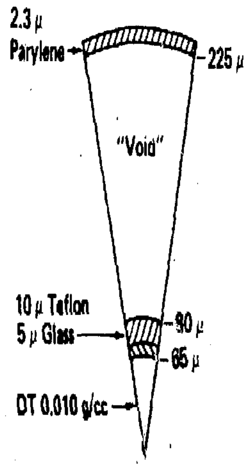

Shiva Laser Illumination

1 ns FWHM Gaussian
7 kilojoules

50-60-1278-4712

Figure 27

After an initial ablation by hot electrons, the fuel ball is driven by the impact from the exploded outer shell.

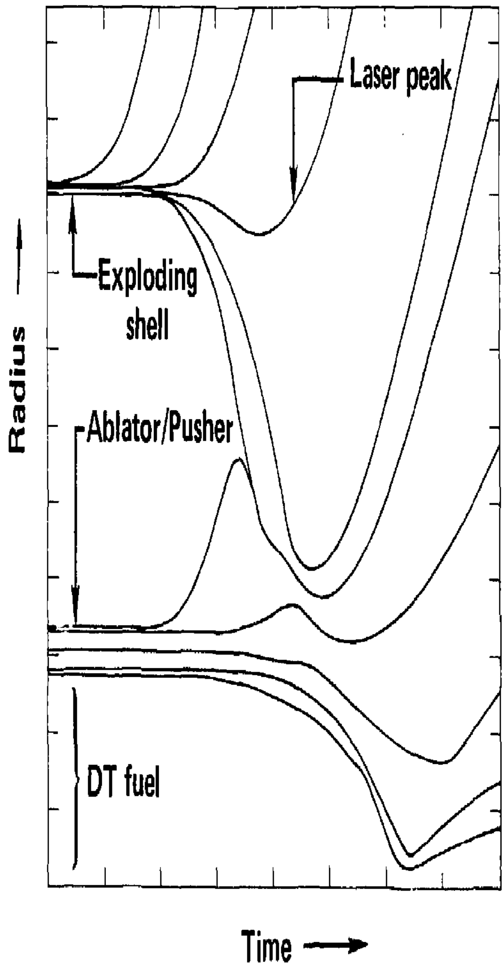

50-60-0978-3293

Figure 28

TRANSITION FROM SINGLE SHELL TO DOUBLE SHELL DYNAMICS

Variation of yield and density with outer shell radius

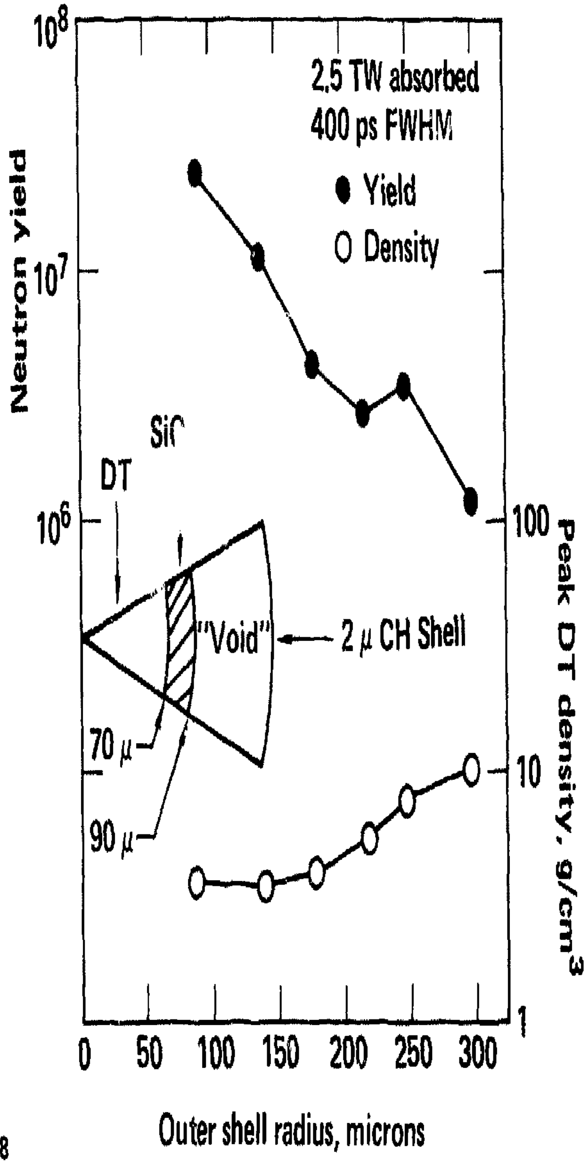

50-60-0779-2248

Figure 29

HYDRODYNAMIC FLOW TENDS TO SYMMETRIZE THE PRESSURE ON THE ABLATOR/PUSHER

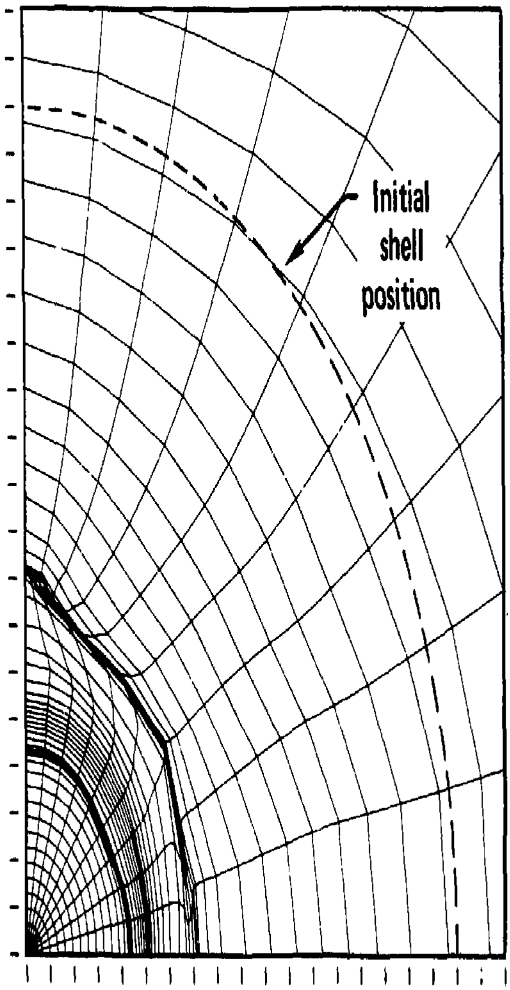

RO=	0.	DSEP2DM2		CYCLE=	600.0
ZO=	0.	DR/DZ=	1.00	TIME=	2.1577E-01
ZMX=	2.5000E-02	PRMX=	1.1949E-02	RHOMX=	8.0507E+00

50-60-027 90589

Figure 30

X-RAY EMISSION COMPARISON – EXPERIMENT AND SIMULATION

Shot # 88111607
3X microscope
1.5 KeV

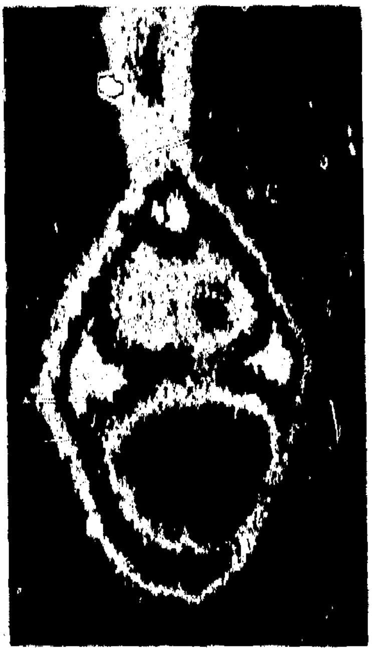

2-D simulation
TDG
1.5 KeV

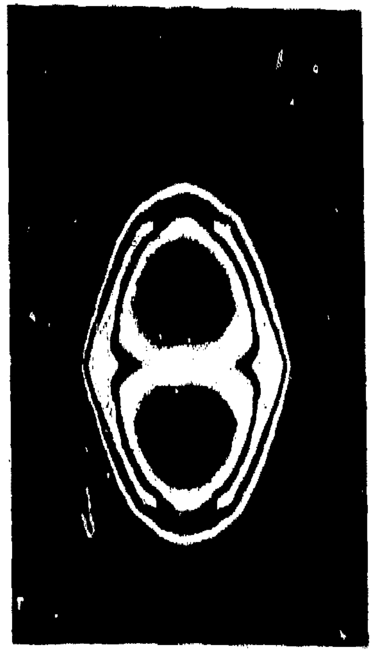

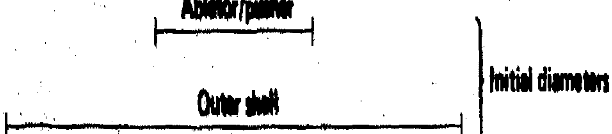

Figure 31

OTHER EXPERIMENTS INDICATE THAT ABSORPTION ON CH AT 1 NS FWHM IS LESS THAN 10%

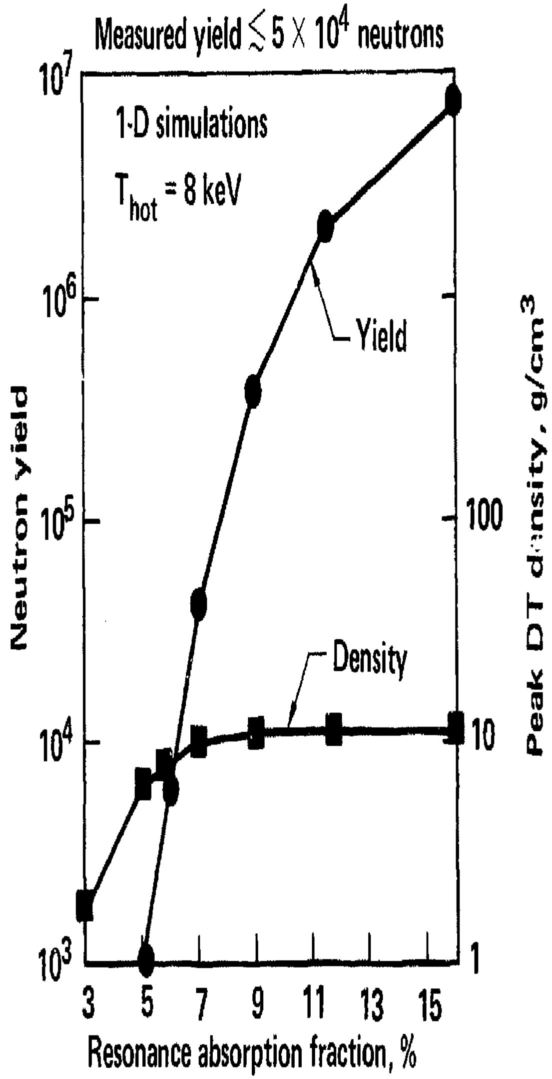

50-60-0779-2258

Figure 32

MAGNETIC FIELDS DEGRADE THE SYMMETRY OF THE ABLATOR/ PUSHER IMPLOSION BUT DO NOT PREVENT FORMATION OF THE RING SHOCK

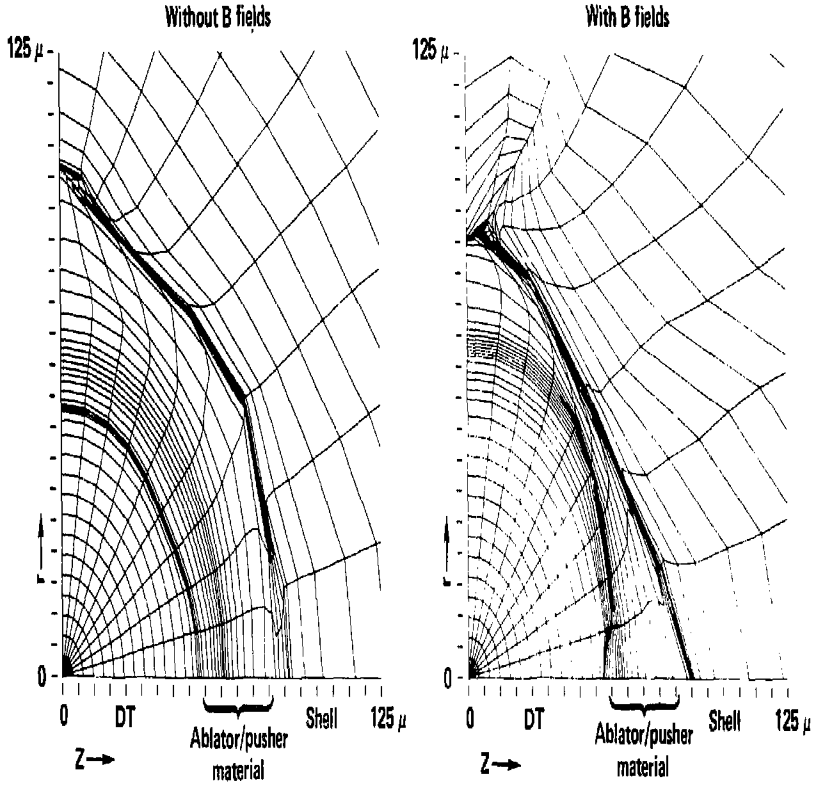

50-60-0279-0590

Figure 33

IMPROVE ABSORPTION AND SYMMETRY BY GOING TO SHORTER LASER PULSE AND THINNER BALL

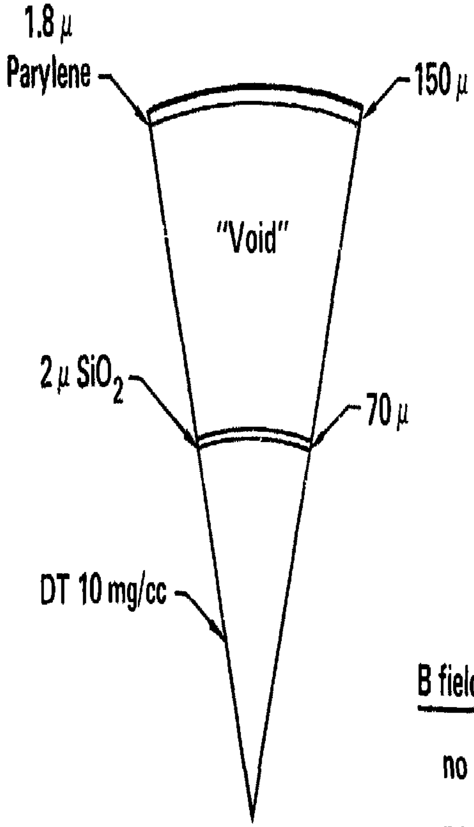

SHIVA laser

200 ps FWHM gaussian

3.6 kilojoules

Observed performance

Yield	Density
$(2.2 \pm 0.4) \times 10^7$	?
$(1.5 \pm 0.3) \times 10^7$	?

Calculated performance (2 – D)

B fields	Inhibition	Yield	Density
no	2-stream	1×10^9	1 X
no	f = 0.03	9×10^8	1 X
yes	none	7×10^8	2 X
yes	2-stream	1.4×10^7	1.5 X

50-60-0779-2255

Figure 34

ASPHERICAL EXPLODING – PUSHER TARGET CAN BE USED TO OBTAIN IMPROVED IMPLOSION SYMMETRY WITH TWO-SIDED ILLUMINATION

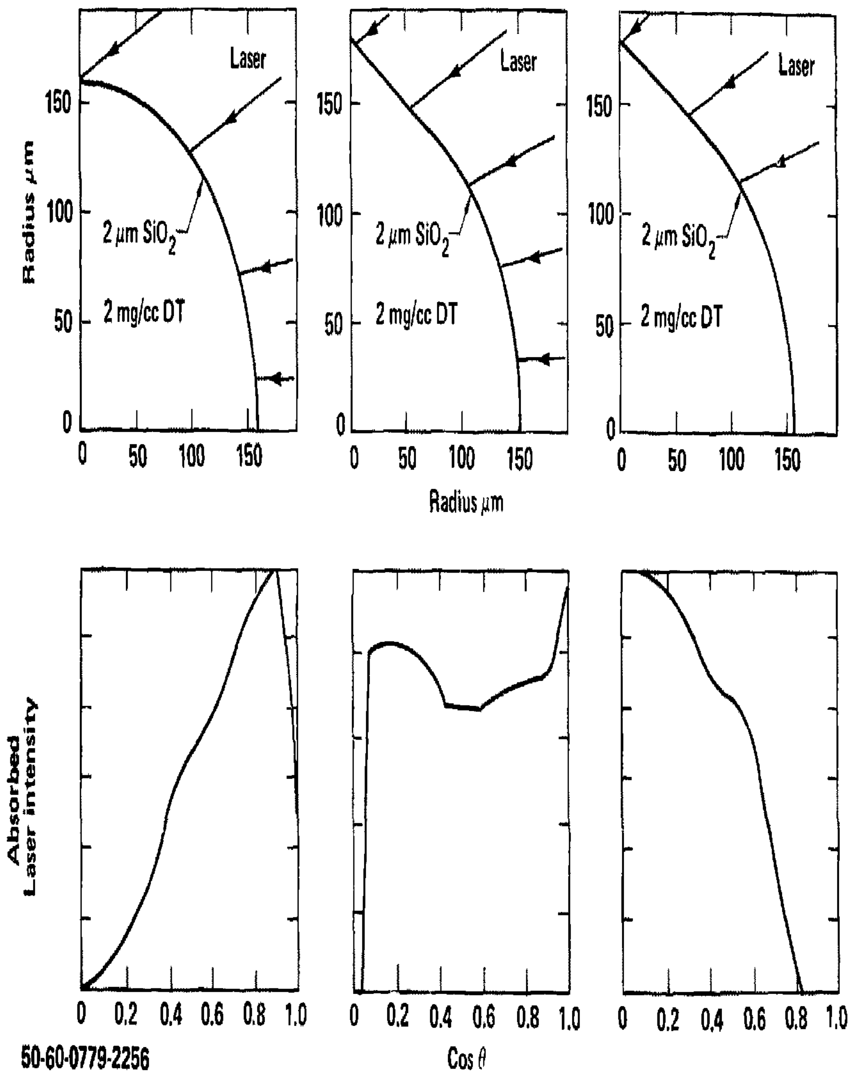

Figure 36

IMPLOSION SHAPE IS VERY SENSITIVE TO LASER ILLUMINATION PROFILE. NEUTRON YIELD REMAINS APPROXIMATELY CONSTANT.

Simulations with 90 ps FWHM gaussian, 19 TW.

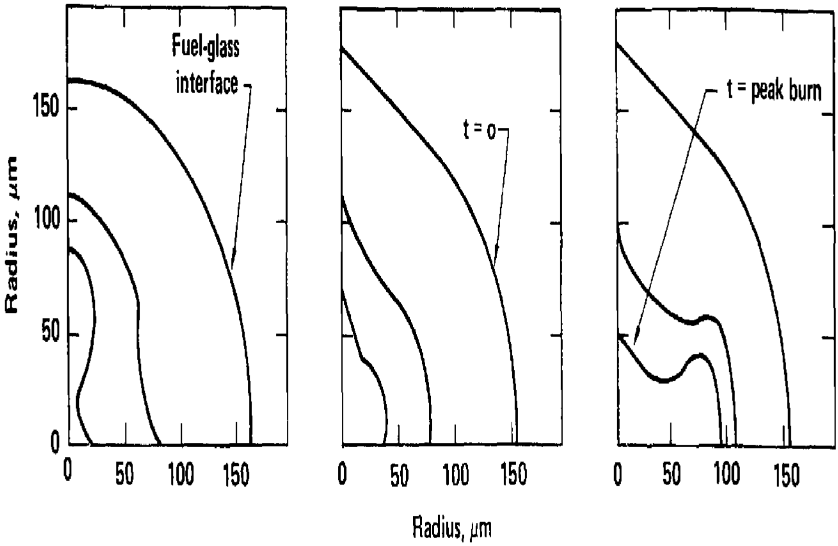

Energy absorbed	288 J	294 J	293 J
Neutron yield	8×10^9	8×10^9	1×10^{10}

50-60-0779-2257

Figure 37

DESIGN CONSIDERATIONS FOR DIAGNOSABLE 10-100X TARGETS

- Implosion matched to available laser pulse length and power
- Radiochemistry
  - Sufficient $N\rho\Delta R$
  - Active atoms in thin layer adjacent to fuel
  - Burn close to peak compression
- Argon line imaging
  - Sufficient T_e to excite line
  - Pusher not too opaque
- X-ray imaging
  - Energy high enough to penetrate pusher

50-60-0879-2343

Figure 38

NEAR-TERM IMPROVEMENTS FOR HIGHER DENSITY

- Improve symmetry
  - Ball-in-plate targets
  - Double-shelled targets
- Reduce preheat
  - Longer pulse length
  - Double-shelled targets
  - Higher-Z pusher
- Improve density diagnostics
  - Thinner glass in pusher
  - Radiochemistry tracer in fuel
  - X-ray backlighting

50-60-0879-2342

Figure 39

SUMMARY

- Dynamics of 10-100X implosions
- Methods of diagnosing peak fuel density
- 10X experiment diagnosed by three methods
- Double-shelled targets – initial work

50-90-0879-2344

Figure 40